

iPOKE: Poking a Still Image for Controlled Stochastic Video Synthesis

Andreas Blattmann^{1,2} Timo Milbich^{1,2} Michael Dorkenwald² Björn Ommer^{1,2}

¹Ludwig Maximilian University of Munich ²IWR, Heidelberg University, Germany

Abstract

How would a static scene react to a local poke? What are the effects on other parts of an object if you could locally push it? There will be distinctive movement, despite evident variations caused by the stochastic nature of our world. These outcomes are governed by the characteristic kinematics of objects that dictate their overall motion caused by a local interaction. Conversely, the movement of an object provides crucial information about its underlying distinctive kinematics and the interdependencies between its parts. This two-way relation motivates learning a bijective mapping between object kinematics and plausible future image sequences. Therefore, we propose iPOKE – invertible Prediction of Object Kinematics – that, conditioned on an initial frame and a local poke, allows to sample object kinematics and establishes a one-to-one correspondence to the corresponding plausible videos, thereby providing a controlled stochastic video synthesis. In contrast to previous works, we do not generate arbitrary realistic videos, but provide efficient control of movements, while still capturing the stochastic nature of our environment and the diversity of plausible outcomes it entails. Moreover, our approach can transfer kinematics onto novel object instances and is not confined to particular object classes. Our project page is available at <https://bit.ly/3dJN4Lf>.

1. Introduction

Imagine a 3-year-old standing next to a stacked pyramid of glasses in a shop. Can you sense the urge to pull one glass out—just to observe what happens. We have an inborn curiosity to understand how the world around us reacts to our actions, so we can eventually imagine and predict their outcome beforehand. This ability to predict is the prerequisite for targeted, goal-oriented interaction with our world rather than random manipulation of our environment. Once we are older, we have also learned to generalize and predict the dynamics of previously unseen objects when they are pulled or poked; and the less audacious have understood that it is often more effective to have others do daring experiments like the one above (and pay the bill) while they are learning by merely watching the outcome. While such experiments

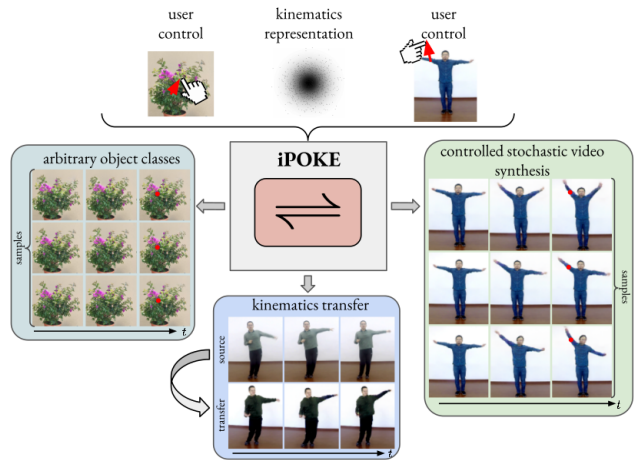


Figure 1. *iPOKE*: Conditioned on a local poke controlling desired object motion in a static image, our invertible model learns a representation of the remaining object kinematics for arbitrary object classes. Once learned, our framework allows users to locally control intended movements while sampling diverse realistic motion for the remainder of the object and to even transfer kinematics to unseen object instances.

are not just fun to watch, they also help to imagine the many possible outcomes caused by the stochastic nature of the many factors beyond our control.

Given a single static image, how can an artificial vision system imagine, i.e. synthesize, the many possible outcomes when locally manipulating the scene? It needs to learn how a local poke affects different parts of an object and the resulting kinematics [49]. Conditioned on only the start frame and the displacement of a single pixel, we want to synthesize multiple videos, each showing the different plausible future dynamics. To render this generative, stochastic approach widely applicable, training should only require videos of objects in motion, but no ground truth information regarding the forces acting on an object such as a local poke. The representation of the kinematics should then generalize to similar objects not seen during training in contrast to instance specific models [15]. Moreover, the method should work for arbitrary objects, rather than being tuned to just a single class [1, 21]. Therefore, no prior motion model is available, but all kinematics have to be learned from the unannotated

video data. Previous work on video synthesis has mainly explored two opposing research directions: (*i*) uncontrolled future frame prediction [24, 10, 53, 59] synthesizing videos based on a start frame, but with no control of scene dynamics, and (*ii*) densely controlled video synthesis [50, 73, 77, 74] demanding tedious, per-pixel guidance how the video will evolve such as by requiring the object motion to be provided per pixel [50, 73, 77] or a future target frame [74]. Our sparsely controlled video synthesis based on few local user interactions constitutes the rarely investigated midground in between, allowing for specific but still efficient control of kinematics.

In this paper, we present a model for exercising local control over the kinematics of objects observed in an image. Indicating movements of individual object parts with a simple mouse drag provides sufficient input for our model to synthesize plausible, holistic object motion. To capture the ambiguity in the global object articulation, we learn a dedicated latent kinematic representation. The synthesis problem is then formulated as an invertible mapping between object kinematics and video sequences conditioned on the observed object manipulation. Due to its stochastic nature, our latent representation allows to sample and transfer diverse kinematic realizations fitting to the sparse local user input to then infer and synthesize plausible video sequences as shown in Fig. 1.

To evaluate our model on controlled stochastic video synthesis, we conduct quantitative and qualitative experiments on four different datasets exhibiting complex and highly articulated objects, such as humans and plants. Comparisons with the state-of-the-art in stochastic and controlled video prediction demonstrate the capability of our model to predict and synthesize plausible, diverse object articulations inferred from local user control.

2. Related Work

Video Synthesis. Video synthesis denotes the general task of generating novel video sequences. While some works solely focus on transferring a predefined holistic motion between objects [73] or interpolating motion between a starting and end frame [54, 79, 43, 4, 55], the most commonly addressed problem is video prediction. Given an initially observed video sequence, the goal is to infer a likely continuation into the future. To this end, proposed methods either generate a single, deterministic video sequence [76, 70, 69, 77, 6] or model the distribution over likely future sequences [23, 16, 40, 59, 53, 10, 19]. Moreover, the employed model architectures exhibit large divergence with latent RNN-based methods being the dominant modelling choice [53, 24]. However, also more complex models based on transformers [75], pixel-level autoregression [51, 40, 45, 16, 70, 10], factorization of dynamics and content [53, 24] and image warping using optical

flow [71, 44, 25] have been proposed. Despite these methods showing promising results, none of them is able to exercise control over the video generation process.

Controllable Video Synthesis. Exercising user control over the video synthesis process requires a detailed understanding of the object kinematics and interplay of the object parts. To circumvent the difficult task of learning object kinematics directly from data, Davis et al. [15] resort to fixed, linear mathematical models. Thus, they can only consider constraint oscillating motion around an object’s rest state. In contrast, our model learns natural, unconstrained object kinematics from video, thus is also applicable to highly complex articulation such as those of humans. Other works rely on a low-dimensional, parametric representation e.g. keypoints to transfer motion between videos [1, 5] or to synthesize videos based on action labels [81]. Given such assumptions, these works cannot be universally applied to arbitrary object categories and allow only for coarse control compared to our fine-grained, local object manipulations. By iteratively warping single images with local sets of estimated optical flow vectors, [27] takes a first step towards sparsely controlled video generation for arbitrary object categories. However, due to the method’s warping based nature, it is still not able to generate temporally coherent motion and requires optical flow guidance for each individual predicted image frame. To overcome such limitations, [6] introduces a hierarchical dynamics model, which can predict complex object dynamics controlled by a single optical flow vector in a given image, but does still not consider the natural motion ambiguity of the remaining, uncontrolled object parts. In contrast, our model learns a dedicated, stochastic kinematics representation modeling this incertitude of the object remainder and, thus, is capable of synthesizing locally controlled but also diverse object motion.

Invertible Neural Networks. Invertible neural networks (INNs) are learnable bijective functions often used to transform between two probability distributions, thus being a natural choice for addressing inverse problems [3], introspecting and explaining neural network representations [22, 32] and domain transfer [62, 63]. Typically, INNs are realized as generative normalizing flows [60, 47, 37] which have recently also found application in image [37, 58] and video synthesis [39, 19]. In this work, we use normalizing flows to learn the missing residual information, i.e. the latent object kinematics, not being determined by the sparse local control over part of the object motion.

3. Approach

Controlled video synthesis seeks to generate a plausible future video sequence $\mathbf{X} \in \mathbb{R}^{T \times H \times W \times 3}$ given an initial frame x_0 and a user-defined control c that locally specifies part of the video dynamics,

$$(x_0, c) \mapsto \mathbf{X} = [x_1, \dots, x_T]. \quad (1)$$

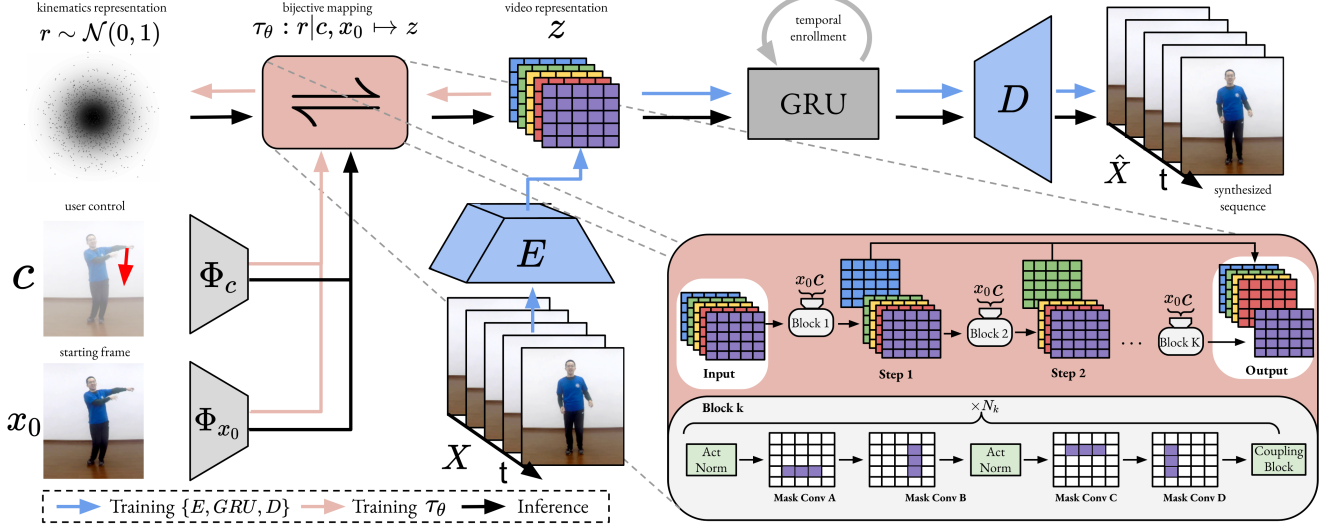


Figure 2. *Overview of our proposed framework iPOKE for controlled video synthesis:* We apply a conditional bijective transformation τ_θ to learn a residual kinematics representation r capturing all video information not present in the user control c defining intended local object motion in an image frame x_0 (orange path). To retain feasible computational complexity, we pre-train a video autoencoding framework (E, GRU, D) (blue path) yielding a dedicated video representation z as training input for τ_θ . Controlled video synthesis is achieved by sampling a residual r , thus defining plausible motion for the remaining object parts not directly affected by c , and generating video sequences \hat{X} from the resulting $z = \tau_\theta(r|x_0, c)$ using GRU and D (black path).

Our goal is here to efficiently control video synthesis. Instead of having users tediously specify the dynamics at each pixel, e.g. by providing a dense vector field [77], c should only be a very sparse signal. Thus, we assume to be provided only a local poke, the desired movement at one image location between start and end frame. The poke $c \in \mathbb{R}^4$ consequently comprises a shift, $c_{1:2}$, at a single pixel location, $c_{3:4}$, performed only by a simple mouse drag. Evidently, even densely defining the motion of every pixel between start and end frame does not fully define the object dynamics in between, even less so only a sparse 4D c vector. Given this highly limited conditioning information, we model the distribution of all plausible future videos

$$\mathbf{X} \sim p(\mathbf{X}|x_0, c), \quad (2)$$

thus contrasting previous work, which only yields some arbitrary, uncontrolled realization [40, 45, 16, 10]. Our main challenge is then to model the *object kinematics* which define how the movement of one part of an object affects the rest, thus yielding overall concerted object dynamics. As \mathbf{X} is a random variable, the mapping in (1) is actually non-unique. There is a lot of residual information r beyond user control, which we need to turn (1) into a unique one-to-one mapping

$$(x_0, c, r) \mapsto \mathbf{X}, \quad (3)$$

where the residual r would then capture object kinematics specifying the movement of the remaining object parts given the sparse local control c .

3.1. Invertible Controlled Video Synthesis

Seeking to find the mapping (3) we naturally arrive at a problem of stochastic video prediction. So far, the dominant approach to such problems are conditional variational autoencoder (cVAE) based models [38, 61, 65]. cVAE employs strong regularization to remove the given conditioning from the remaining data variations, thus facing a *trade-off* between synthesis quality and capturing all these variations [11, 83], in our case the diverse object kinematics r . To avoid this, we use a conditional bijective, i.e. one-to-one, mapping τ between each residual r and the corresponding video

$$\mathbf{X} = \tau(r|x_0, c) \quad (4)$$

so that all plausible \mathbf{X} for a given conditioning can be synthesized. Moreover, the inverse mapping τ^{-1} allows to recover the residual kinematics for any \mathbf{X} ,

$$r = \tau^{-1}(\mathbf{X}|x_0, c), \quad (5)$$

which then can be considered as a random variable $r \sim p(r|x_0, c)$, since τ^{-1} is unique and \mathbf{X} is a random variable defined in (2). To solve the conditional video synthesis task, we now show how to learn τ such that r (i) indeed contains all video information not present in (x_0, c) and (ii) follows a distribution which can be easily sampled from.

Learning the invertible mapping τ . We equip τ with parameters θ which, by employing Eq. (5), can be learned from training videos \mathbf{X} . By the change-of-variables theorem for

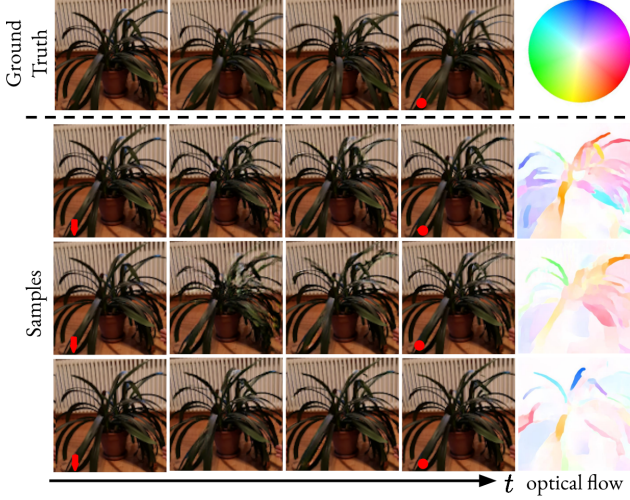


Figure 3. Controlled stochastic video synthesis showing three video sequences for the same user control c (red arrow) and randomly sampled kinematics r on the PP dataset. Our model generates diverse, plausible object motion while accurately approaching the target location (red dot) for the controlled object part. Additionally, to ease comparison of the motion difference between samples, we show optical flow maps between the first and last frame of each sequence. Best viewed in video on our [project page](#).

probability distributions, we have

$$\begin{aligned} p(\mathbf{X}|x_0, c) &= \frac{p(\tau_\theta(r|x_0, c)|x_0, c)}{|\det J_{\tau_\theta}(r|x_0, c)|} \\ &= p(\tau_\theta^{-1}(\mathbf{X}|x_0, c)|x_0, c) \cdot |\det J_{\tau_\theta^{-1}}(\mathbf{X}|x_0, c)|. \end{aligned} \quad (6)$$

Here, J_{τ_θ} denotes the Jacobian of the transformation τ_θ and $|\det[\cdot]|$ the absolute value of the determinant. Recall that we have to ensure to learn τ_θ such that r contains all video information *not* present in (x_0, c) . Effectively, this requires learning τ_θ such that r is independent of (x_0, c) . This can be achieved by introducing some independent prior $q(r)$ and minimizing $\text{KL}[p(r|x_0, c)\|q(r)]$, which then constitutes an upper bound on the mutual information $\text{MI}[r, (x_0, c)]$ [2, 62] as derived in Appendix D.1 and thus, indeed forces the intended independence. Moreover, by using Eq. (5) and (6), we can express $\text{KL}[p(r|x_0, c)\|q(r)]$ as a function of the training data \mathbf{X} what facilitates learning of τ_θ by minimizing

$$\text{KL}[p(r|x_0, c)\|q(r)] \propto \mathbb{E}_{\mathbf{X}} \left[-\log (q(\tau_\theta^{-1}(\mathbf{X}|x_0, c))) - \log |\det J_{\tau_\theta^{-1}}(\mathbf{X}|x_0, c)| \right]. \quad (7)$$

By selecting $q(r) = \mathcal{N}(r|0, \mathbf{I})$ [38, 80] and inserting this into Eq. (7) we arrive at the simple objective function

$$\begin{aligned} \min_{\theta} \mathcal{L}(\tau_\theta, \mathbf{X}, x_0, c) &= \mathbb{E}_{\mathbf{X}, x_0, c} [\|\tau_\theta^{-1}(\mathbf{X}|x_0, c)\|_2^2 \\ &\quad - \log |\det J_{\tau_\theta^{-1}}(\mathbf{X}|x_0, c)|]. \end{aligned} \quad (8)$$

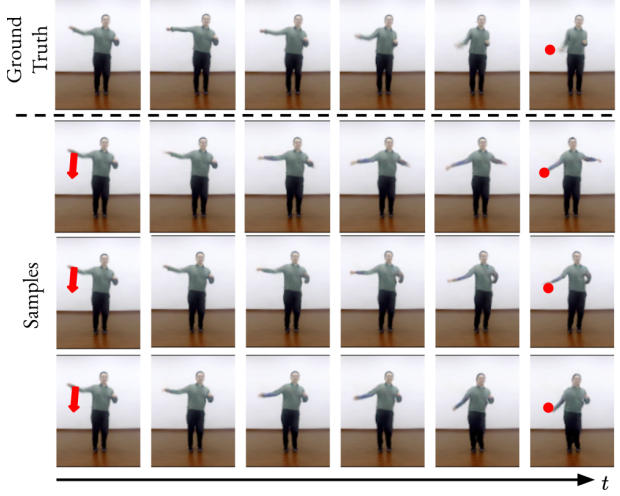


Figure 4. Controlled stochastic video synthesis showing three video sequences for the same user control c (red arrow) and randomly sampled kinematics r on the iPER dataset. Our model generates diverse, plausible object motion while accurately approaching the target location (red dot) for the controlled body part. Best viewed in video on our [project page](#).

A detailed derivation can be found in the Appendix D.2. Note, that optimizing Eq. (8) *simultaneously* ensures (i) independence of r and (x_0, c) and (ii) yields a generative probabilistic model as we can easily draw samples from $q(r)$ and use the conditional mapping (4) to obtain synthesized videos. Thus, our model is capable to synthesize videos in a controlled but nonetheless stochastic manner without facing the trade-off encountered in cVAE.

3.2. Architecture for Tractably Learning τ_θ

To realize the conditionally bijective nature of our mapping τ_θ , we implement it as a conditional invertible neural network (cINN) [56, 18, 17, 62, 19], which requires equal dimensionality of the transformed random variables. Thus, \mathbf{X} would demand r to be very high dimensional, entailing infeasible computational complexity. As a remedy, we replace \mathbf{X} with a compact, information-preserving video encoding $z \in \mathbb{R}^{h \times w \times d}$, with $h \cdot w \cdot d \ll H \cdot W \cdot 3 \cdot T$, learned by a standard sequence autoencoding framework [38] consisting of a 3D-ResNet [28] encoder E , a GRU [12] for temporal enrollment in the latent space, and an image decoder G to obtain video predictions $\hat{\mathbf{X}}$. Prior to learning τ_θ , we train this model to reconstruct training videos \mathbf{X} by using a respective loss \mathcal{L}_{rec} and additionally add static and temporal discriminators [13, 73], \mathcal{D}_S and \mathcal{D}_T , to increase visual and temporal coherence of $\hat{\mathbf{X}}$, thus resulting in the objective

$$\mathcal{L}_{ae} = \mathcal{L}_{rec} + \mathcal{L}_{\mathcal{D}_S} + \mathcal{L}_{\mathcal{D}_T}. \quad (9)$$

Detailed information on implementation and training can be found in the Appendix E.1. Afterwards we can learn τ_θ from the compact latent video encodings $z = E(\mathbf{X})$ instead of high-dimensional videos \mathbf{X} .

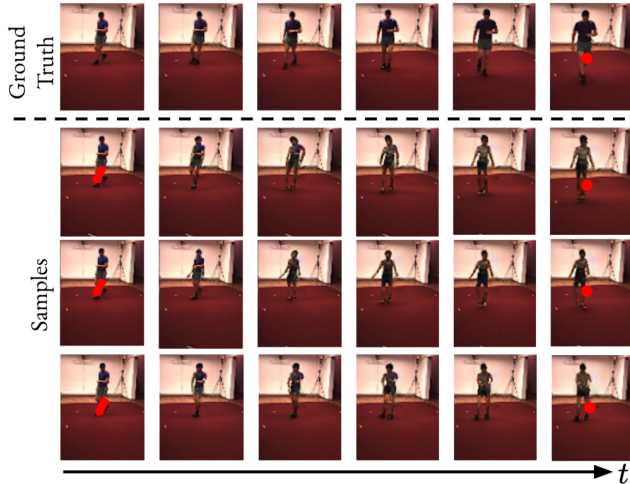


Figure 5. Controlled stochastic video synthesis showing three video sequences for the same user control c (red arrow) and randomly sampled kinematics r on the Human3.6m dataset. Our model generates diverse, plausible object motion while accurately approaching the target location (red dot) for the controlled body part. Best viewed in video on our [project page](#).

So far, cINNs operating on latent representations have been implemented as a sequence of fully connected layers [32, 62, 63], thus discarding the spatial information naturally constituting visual data. However, since the conditioning c describes a spatial shift of a single pixel, such architectures are not able to effectively leverage this information. To this end, we use the poke c to define a two-channel map $C \in \mathbb{R}^{H \times W \times 2}$ with $C_{c_3, c_4, 1:2} = c_{1:2}$ and zeros elsewhere, and instead design a fully convolutional cINN, such that the crucial spatial information about the control location can be incorporated as best as possible. More specifically, our architecture comprises K subsequently arranged cINN sub-blocks. By directly forwarding a portion $\frac{d}{K}$ of the output of each block to the final representation r , we reduce memory requirements and avoid vanishing gradients for large K [18, 48]. Within the k -th block, we apply a series of N_k masked convolutions [48], which have been shown to obtain improved expressivity compared to standard flow architectures such as coupling layers [17, 18, 37]. Finally, the conditioning information (x_0, c) is separately processed by two dedicated encoding networks Φ_{x_0} and Φ_c , yielding representations of the same spatial size than the flow input, to which they are concatenated before each masked convolution. We visualize the architecture and training in Fig. 2 and provide further details in Appendix E.2.

3.3. Automatic Simulation of User Control

Training our model for controlled video synthesis relies on user controls c and corresponding video sequences X depicting natural object responses to be available. Providing sufficient amounts of such training data for every targeted object category is tedious and costly. Instead, we employ an efficient self-supervised strategy to artificially generate such

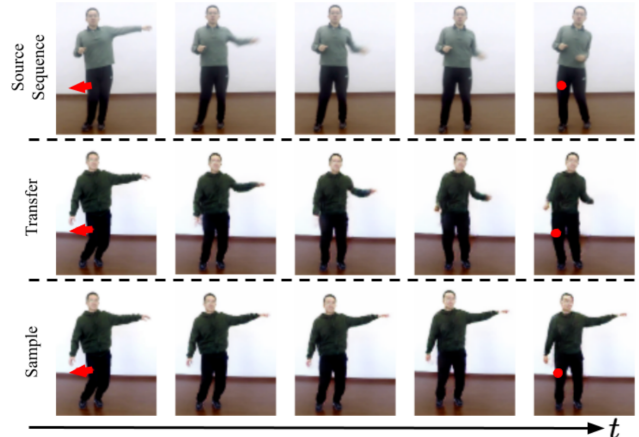


Figure 6. *Motion Transfer on iPER*: We extract the residual kinematics from a ground truth sequence (top row) and use it together with the corresponding control c (red arrow) to animate an image x_t showing similar initial object posture (second row). We also visualize a random sample from $q(r)$ for the same (x_t, c) (bottom row), indicating that the residual kinematics representation solely contains motion information not present in (x_t, c) (for a detailed description cf. Sec. 4.2). Best viewed in video on our [project page](#).

interactions directly from the observed motion of a collection of cheaply available training videos X . To this end, we extract dense optical flow maps [29] $F \in \mathbb{R}^{H \times W \times 2}$ between the start and end frames, x_0 and x_T , of X whose individual shift vectors can be interpreted as sparse pixel displacements $c = \{(F_{l_{n,1}, l_{n,2}, 1}, F_{l_{n,1}, l_{n,2}, 2})\}_{n=1}^{N_c}$. During training, we randomly sample such simulated pokes at positions l_n which exhibit sufficiently large motion that reliably corresponds to the foreground object. Contrasting [6], which use a similar strategy, but restrict the user control to be defined by only a single poke, we allow a user to control the degree of freedom of the object articulation by training our model on up to 5 simultaneous interactions c , i.e. on a variable number $N_c \in [1, 5]$ of local pokes. Note that for inferring user controls after training we do not require optical flow estimates, but use simple mouse drags instead.

4. Experiments

Subsequently, we evaluate our model for controlled stochastic video synthesis on four video datasets showing diverse and articulated object categories of humans and plants. Implementation details and video material can be found in the Appendices F and G, and on our [project page](#).

4.1. Datasets

We evaluate our approach to understand and synthesize object dynamics on the following four datasets:

Poking-Plants (PP) [6] consists of 27 videos of 13 different types of pot plants. To learn a single kinematics model for all plants is notably challenging given the large variance in shape and texture of the plants. Overall, PP contains of 43k frames, from which a fifth is used as a test set and the

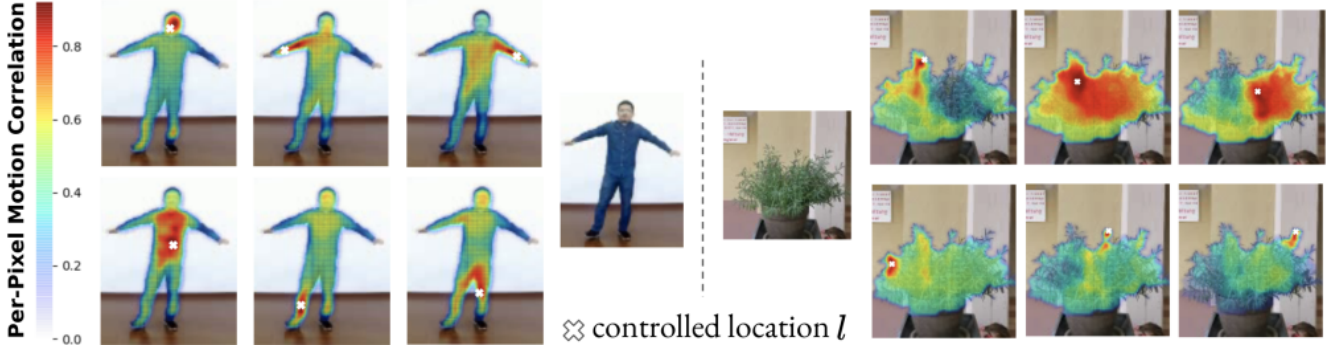


Figure 7. *Understanding object kinematics*: By sampling 1000 random control inputs at location $l = c_{3:4}$ for a fixed image x_0 we obtain varying video sequences, from which we compute motion correlations for l with all remaining pixels. By mapping these correlations to the pixel space, we visualize the interplay correlation of distinct object parts, thus yielding insights about the learned kinematics.

remainder as training data.

iPER [42] contains of 30 humans with diverse styles performing various simple and complex movements. We follow the official train/test split which results in a training set of 180k frames and a test set of 49k frames.

Tai-Chi-HD [64] is a collection of 280 in-the-wild Tai-Chi videos from Youtube. We follow previous work [64] and use 252 videos for training and 28 videos for testing. Given the large variance in background and camera movement, this dataset tests the real-world applicability of our model. Since the motion between subsequent frames is often small, we skip every other frame.

Human3.6m [30] is a large scale human motion dataset with video sequences of 7 human actors performing 17 different actions. We follow previous work [76, 53, 24] by center-cropping and downsampling the videos to 6.25 Hz and by using actors S1,S5,S6,S7 and S8 (600 videos) for training and actors S9 and S11 (239 videos) for testing.

4.2. Qualitative Evaluation

Controlled Stochastic Video Synthesis. In Fig. 3, 4 and 5 we show examples for controlled stochastic video synthesis generated by our proposed model on the PP, iPER and Human3.6m datasets. For each dataset, we show the ground-truth frames following a fixed given image x_0 , as well as three synthesized examples generated from a fixed user control c (red arrows) and randomly sampled kinematics realizations $r \sim q(r)$. Examples for the Tai-Chi dataset can be found in the supplemental, where we also show additional synthesized videos based on control inputs from real human users and demonstrate our model to also plausibly react to different pokes at the same location. The individual videos are discussed in the Appendices A and B.

Transfer of Kinematics. Besides sampling plausible object kinematics, we can also apply our model to transfer the kinematics inferred from a source sequence $\mathbf{X}_s = [x_{s,0}, \dots, x_{s,T}]$ to a novel object instance. To this end, we extract the corresponding residual kinematics $r_s = \tau_\theta^{-1}(\mathbf{X}_s | x_{s,0}, c)$ for a user control c simulated based on \mathbf{X}_s and use Eq. (4) to animate a target image x_t show-

ing another object instance than $x_{s,0}$ with similar articulation. The resulting successfully transferred motion sequence $\hat{\mathbf{X}}_t = \tau_\theta(r_s | x_t, c)$ is shown in Fig. 6 (second row) and compared to \mathbf{X}_s (top row). It can be seen, that the motion contained in \mathbf{X}_s is transferred to $\hat{\mathbf{X}}_t$ but *not* the object appearance shown in $x_{0,s}$, indicating that our model indeed has learned a residual representation r solely containing kinematics. Additionally, we visualize a synthesized video sequence based on a random sample $r \sim q(r)$ of residual kinematics for the same conditioning (x_t, c) (bottom row), showing substantially different object motion except for the controlled body part and thereby providing evidence that r is also independent of the user-control c . More results of kinematics transfer can be found in Appendix A.2.

Understanding Object Kinematics. To demonstrate how well our model captures holistic object kinematics we analyze its understanding of the interplay of integral object parts. Therefore, we measure the pixel-wise correlations when applying 1000 randomly sampled user controls c at a fixed location l of a fixed image x_0 , i.e. varying only direction and magnitude of the shift vector. To measure the correlation in motion of all pixels with respect to the fixed control location (and thus the remaining object parts with the controlled part), we first compute optical flow maps between the start frame x_0 and the end frame x_T of all resulting synthesized video sequences. Next, we compute the shift of the tracked pixel locations in x_T with respect to the interaction location l , thus obtaining 1000 [magnitude, angle] representations of the individual shifts. To measure the correlation of a pixel with l , we now compute the variance over these shifts. Fig. 7 illustrates the resulting correlation maps given different locations l for both humans and plants. For humans, we obtain high correlations for pixels constituting a certain body parts and to parts which are naturally connected to l , showing our model correctly understands the body structure. For the plant, we see pulling at locations close to the trunk (top mid and right) intuitively affects large parts of the object. Interacting with individual small leaves mostly has only little effect on the remaining object, in contrast to the pixels

Method	PP [6]			iPER [42]			Tai-Chi [64]			Human3.6m [30]		
	FVD ↓	LPIPS ↓	SSIM ↑	FVD ↓	LPIPS ↓	SSIM ↑	FVD ↓	LPIPS ↓	SSIM ↑	FVD ↓	LPIPS ↓	SSIM ↑
Hao [27]	361.51	0.16	0.72	235.08	0.11	0.88	341.79	0.12	0.78	259.92	0.10	0.93
Hao [27] w/ KP	—	—	—	141.07	0.04	0.93	—	—	—	—	—	—
I2V [6]	174.18	0.10	0.78	220.34	0.07	0.89	167.94	0.12	0.78	129.62	0.08	0.91
iPOKE (Ours)	63.06	0.06	0.69	77.50	0.06	0.87	100.69	0.08	0.74	119.77	0.06	0.93

Table 1. Comparison with recent methods for sparsely controlled video synthesis [27, 6].

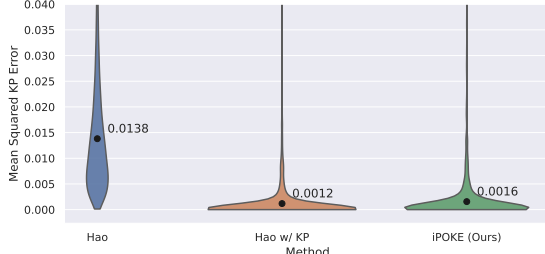


Figure 8. *Control accuracy*: On the iPER dataset, we extract control signals c based on ground truth keypoints and also estimate keypoints for the resulting synthesized videos. We only evaluate the errors with respect to those keypoints used to define c . The violins show the resulting MSE distributions. The numbers are the mean errors in keypoint space indicated by the black dots. Our model outperforms the baselines of Hao et al. by a large margin and even approaches their model which is trained on keypoints.

representing the leave.

4.3. Quantitative Evaluation

As our proposed task of controlled *and* stochastic video synthesis has been so far unattempted, we cannot directly compare iPOKE to previous work. To nevertheless quantitatively prove our model to reliably achieve this task, we separately compare against the current state of the art stochastic video prediction models [40, 10, 24] and sparsely controlled video synthesis approaches [27, 6]. For all competitors we used the provided pretrained models, where available, or trained the models using official code.

Evaluation Metrics

Motion Consistency. We evaluate the synthesis quality by using the Fréchet Video Distance [68] (FVD, lower-is-better) which is responsive to visual as well as temporal coherence and uses an I3D network [67] trained on the Kinetics [34] dataset as backbone. Unterthiner et al. [68] showed that the metric correlates well with human judgement. The FVD-scores we report are obtained from video of length 10.

Synthesis Quality. Since we have no direct means to evaluate how well iPOKE models object kinematics, we compare its synthesized videos against the groundtruth using two commonly used framewise metrics, as producing uncorrect kinematics would lead to large errors between the individual generated and groundtruth frames. We average over time and over 5 samples due to the stochastic nature of our model. As it has been shown to account for high- and low-frequency image differences and also to correlate well with human judgement, LPIPS [82] (lower-is-better) is the metric of choice for this task. Additionally, due to its wide application, we report framewise discrepancy as measured by SSIM [84]. However, as this metric compares image patches

based on the L2 distance, it is known to be deceivable by blurry predictions.

Motion Diversity. Following previous work [40, 85] we evaluate the diversity by computing mutual distances between the individual frames of different video samples (while fixing the user control) using the LPIPS [82] metric. Moreover, we also directly evaluate the diversity in the pixel space using the MSE, thus measuring low-frequency image differences.

Controllable Video Synthesis. We compare our model with the considered methods for sparsely controlled video synthesis [27, 6] on all considered datasets using LPIPS [82], SSIM [84] and FVD [68] on images of resolution of 128×128 . Note that both competing baselines are limited in that they provide no means to stochastically model the inherent ambiguity of the non-controlled object parts. Additionally, [27] lacks a dedicated dynamics model, as this method is based on a warping technique, which we describe in Appendix F, and requires more than one control inputs to reliably generate complex object articulation. Due to these limitations, our model exhibits significantly better temporal and visual consistency as indicated by the large gaps in FVD and LPIPS scores in Tab. 1. To provide a stronger baseline, we also train and evaluate the model of Hao et al. with input trajectories based on groundtruth keypoints (Hao w/KP) which are readily available for the iPER dataset and much more reliable than those based on estimated optical flow. Despite this advantage, we also outperform this baseline in FVD and generate similarly sharp image frames as indicated by comparable LPIPS scores.

Next, we use the displacements between the groundtruth keypoints of the test sequences to construct targeted user controls for each individual part of the human body. By using these manipulations as test-time inputs and estimating keypoints [66] for the resulting generated videos, we assess the targeted control accuracy by measuring the Mean Squared Error (MSE) only between those estimated and groundtruth keypoints which correspond to the poked body parts. Fig. 8 shows the resulting error distributions and means (black dots) showing that we significantly outperform Hao et al. [27] and achieve similar performance to their keypoint-based version. Thus our model allows for accurate control of body parts which are correctly moved to the intended target locations.

Stochastic Video Synthesis. To evaluate the visual quality and the diversity of generated videos we compare against recent state of the art methods for stochastic video synthesis (SVS) [40, 53, 24], each of them based on variational autoencoder (VAE). We adopt the SVS evaluation protocol and generate videos of spatial size 64×64 . Tab. 2

Method	PP			iPER [42]			Tai-Chi [64]			Human3.6m [30]		
	FVD ↓	DIV MSE [‡] ↑	DIV LPIPS [‡] ↑	FVD ↓	DIV MSE [‡] ↑	DIV LPIPS [‡] ↑	FVD ↓	DIV MSE [‡] ↑	DIV LPIPS [‡] ↑	FVD ↓	DIV MSE [‡] ↑	DIV LPIPS [‡] ↑
SAVP [40] [†]	92.2	—	—	92.8	—	—	236.8	—	—	131.7	—	—
IVRNN [10]	128.3	2.52	8.23	126.0	37.66	93.26	150.2	0.34	1.65	238.6	46.45	106.71
SRVP [24]	171.9	110.37	225.77	274.2	53.94	164.46	268.9	30.2	16.00	140.1	93.61	224.07
iPOKE (Ours)	56.59	133.37	275.04	81.49	98.95	201.58	96.09	69.96	126.76	111.55	124.25	309.06

Table 2. Comparison with recent state-of-the-art in stochastic video prediction. As our model does not face trade-off between variability and synthesis quality, we obtain significantly better motion video quality and diversity scores for all considered datasets. [†]: SAVP faced mode collapse due to training instabilities caused by the two involved discriminator networks. As a consequence their model generates entirely equal outputs when sampling. Therefore, we are unable to report diversity scores for this baseline. [‡]: Reported numbers multiplied with $1e-4$.

summarizes the comparison in video quality (measured in FVD score) and sample diversity (measured using LPIPS and pixel-space MSE). All SVS methods are conditioned on two image frames directly preceding the predicted sequence if not stated otherwise. Details for training and evaluation protocols can be found in the Appendices F and G. Our method outperforms all competing approaches by large margins in both video quality and diversity. Moreover, Tab. 2 reveals that competing methods which achieve comparable FVD scores to ours, i.e. video synthesis of similar visual quality, fail in generating diverse samples and vice versa. We attribute the limited performance of these models to the discussed trade-off in synthesis quality and capturing data variations of VAE-based approaches (cf. Sec. 3.1).

Controlling Future Ambiguity. We now assess the ability of our model to control the degree of freedom in stochastic object articulation by varying the number of local pokes. Intuitively, an increasing number of user controls should result in more accurate predictions and lowered between-sample-variance due to the reduction in future ambiguity. We evaluate the amount of uncertainty in predictions by comparing average reconstruction scores of a fixed number of samples from $q(r)$ for increasing numbers of user controls. More specifically, we report the mean prediction error and standard deviation of 50 samples (Std-50s) for each of 1000 input images and pokes. On the iPER dataset this is done by measuring MSE between estimated [66] and groundtruth keypoints. For PP dataset we resort to the LPIPS metrics as keypoints are not available. The resulting curves are depicted in Fig. 9. As expected, the decreasing prediction errors and between-sample-variances indicate that our model leverages the additional future information provided by an increased number of pokes. Thus, our model not only generates diverse predictions but also provides means to control their uncertainty by choosing an appropriate number of input pokes.

Ablation Study. As the competing VAE-grounded baselines for SVS are all conditioned on observed motion in form of observed past frames rather than dedicated, local user control, we further compare our model method to a cVAE-baseline (Ours cVAE) for locally controlled video synthesis. Thus, we use the exact architecture of our video-autoencoding framework (cf. Sec. 3.2) except for our latent cINN model. To enable sampling, we realize the latent video representation z as a gaussian distribution and regularize it towards a standard normal prior. The encodings obtained from the control c and source image x_0 are concatenated with z and

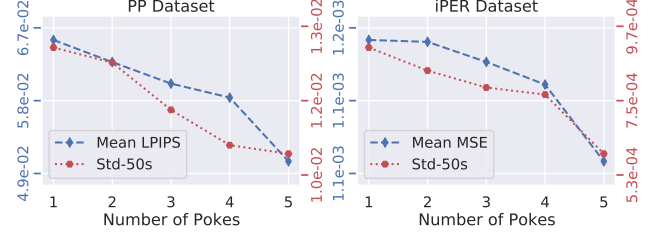


Figure 9. *Controlling Future Ambiguity*: On the PP (left) and iPER (right) datasets our model reduces mean prediction errors (blue) and standard deviations of a sample of 50 residual samples given the same (x_0, c) for an increased number of control inputs. Thus, our approach enables users to control future ambiguity by selecting the number of control inputs.

Method	PP			Human3.6m [30]		
	FVD ↓	DIV MSE ↑	DIV LPIPS ↑	FVD ↓	DIV MSE ↑	DIV LPIPS ↑
Ours cVAE	70.9	3.37	7.59	269.6	83.17	210.39
iPOKE (Ours)	56.59	133.37	275.04	111.55	124.25	309.06

Table 3. *Ablation*. Comparison with a cVAE-counterpart to our cINN-based model for controlled video synthesis, indicating its superior performance due to variability vs. quality trade-off in cVAE.

constitute the hidden state for the latent GRU. A detailed architecture and training description of the baseline is contained in the Appendix F. Thus, this baseline is the exact variational counterpart of our model. We conduct ablation experiments on all the considered object categories, using the PP and Human3.6m datasets. Tab. 3, which summarizes the results, again indicates the improved performance of our invertible model compared to variational approaches.

5. Conclusion

We presented a novel model for controlling and synthesizing object kinematics of arbitrary object categories by locally manipulating object articulation using simple mouse drags. Our model is based on an invertible mapping between the generated video sequences and a dedicated kinematics representation learned from training videos only. To account for the ambiguity in the global object articulation given a local shift determining the motion of only an object part, learning is based on a probabilistic formulation, thus allowing us to sample and synthesize diverse kinematic realizations.

Acknowledgements

This research is funded in part by the German Federal Ministry for Economic Affairs and Energy within the project KI-Absicherung Safe AI for automated driving and by the German Research Foundation (DFG) within project 421703927.

References

- [1] Kfir Aberman, Yijia Weng, Dani Lischinski, Daniel Cohen-Or, and Baoquan Chen. Unpaired motion style transfer from video to animation. *ACM Transactions on Graphics (TOG)*, 39(4):64, 2020. [1](#), [2](#)
- [2] Alexander A. Alemi, Ian Fischer, Joshua V. Dillon, and Kevin Murphy. Deep variational information bottleneck. *CoRR*, 2016. [4](#), [16](#), [17](#)
- [3] Lynton Ardizzone, Jakob Kruse, Carsten Rother, and Ullrich Köthe. Analyzing inverse problems with invertible neural networks. In *Int. Conf. Learn. Represent.*, 2019. [2](#)
- [4] Wenbo Bao, Wei-Sheng Lai, Chao Ma, Xiaoyun Zhang, Zhiyong Gao, and Ming-Hsuan Yang. Depth-aware video frame interpolation. In *IEEE Conf. Comput. Vis. Pattern Recog.*, pages 3703–3712, 2019. [2](#)
- [5] Andreas Blattmann, Timo Milbich, Michael Dorkenwald, and Björn Ommer. Behavior-driven synthesis of human dynamics. In *Proceedings of the IEEE/CVF Conference on Computer Vision and Pattern Recognition (CVPR)*, pages 12236–12246, June 2021. [2](#)
- [6] Andreas Blattmann, Timo Milbich, Michael Dorkenwald, and Björn Ommer. Understanding object dynamics for interactive image-to-video synthesis. In *Proceedings of the IEEE/CVF Conference on Computer Vision and Pattern Recognition (CVPR)*, pages 5171–5181, June 2021. [2](#), [5](#), [7](#), [19](#)
- [7] Andrew Brock, Jeff Donahue, and Karen Simonyan. Large scale GAN training for high fidelity natural image synthesis. In *Int. Conf. Learn. Represent.*, 2019. [17](#)
- [8] J. Carreira and A. Zisserman. Quo vadis, action recognition? a new model and the kinetics dataset. In *2017 IEEE Conference on Computer Vision and Pattern Recognition (CVPR)*, 2017. [20](#)
- [9] João Carreira and Andrew Zisserman. Quo vadis, action recognition? A new model and the kinetics dataset. In *IEEE Conf. Comput. Vis. Pattern Recog.*, pages 4724–4733, 2017. [20](#)
- [10] L. Castrejon, N. Ballas, and A. Courville. Improved conditional vrnn for video prediction. In *2019 IEEE/CVF International Conference on Computer Vision (ICCV)*, 2019. [2](#), [3](#), [7](#), [8](#), [15](#), [19](#)
- [11] Xi Chen, Diederik P. Kingma, Tim Salimans, Yan Duan, Prafulla Dhariwal, John Schulman, Ilya Sutskever, and Pieter Abbeel. Variational lossy autoencoder. In *Int. Conf. Learn. Represent.*, 2017. [3](#), [20](#)
- [12] Junyoung Chung, Caglar Gulcehre, KyungHyun Cho, and Yoshua Bengio. Empirical evaluation of gated recurrent neural networks on sequence modeling, 2014. cite arxiv:1412.3555Comment: Presented in NIPS 2014 Deep Learning and Representation Learning Workshop. [4](#), [17](#)
- [13] Aidan Clark, Jeff Donahue, and Karen Simonyan. Adversarial video generation on complex datasets, 2019. [4](#), [17](#)
- [14] Djork-Arné Clevert, Thomas Unterthiner, and Sepp Hochreiter. Fast and accurate deep network learning by exponential linear units (elus). In *4th International Conference on Learning Representations, ICLR 2016, San Juan, Puerto Rico, May 2-4, 2016, Conference Track Proceedings*, 2016. [18](#)
- [15] Abe Davis, Justin G. Chen, and Frédo Durand. Image-space modal bases for plausible manipulation of objects in video. *ACM Trans. Graph.*, 2015. [1](#), [2](#)
- [16] Emily Denton and Rob Fergus. Stochastic video generation with a learned prior. In Jennifer G. Dy and Andreas Krause, editors, *International Conference on Machine Learning*, pages 1182–1191, 2018. [2](#), [3](#)
- [17] Laurent Dinh, David Krueger, and Yoshua Bengio. NICE: non-linear independent components estimation. In Yoshua Bengio and Yann LeCun, editors, *Int. Conf. Learn. Represent.*, 2015. [4](#), [5](#), [18](#)
- [18] Laurent Dinh, Jascha Sohl-Dickstein, and Samy Bengio. Density estimation using real NVP. In *Int. Conf. Learn. Represent.*, 2017. [4](#), [5](#), [18](#)
- [19] Michael Dorkenwald, Timo Milbich, Andreas Blattmann, Robin Rombach, Konstantinos G. Derpanis, and Björn Ommer. Stochastic image-to-video synthesis using cnns. In *Proceedings of the IEEE/CVF Conference on Computer Vision and Pattern Recognition (CVPR)*, pages 3742–3753, June 2021. [2](#), [4](#)
- [20] Alexey Dosovitskiy and Thomas Brox. Generating images with perceptual similarity metrics based on deep networks. In Daniel D. Lee, Masashi Sugiyama, Ulrike von Luxburg, Isabelle Guyon, and Roman Garnett, editors, *Adv. Neural Inform. Process. Syst.*, pages 658–666, 2016. [17](#)
- [21] Patrick Esser, Johannes Haux, Timo Milbich, and Björn Ommer. Towards learning a realistic rendering of human behavior. In *ECCV Workshops*, pages 409–425, 2018. [1](#)
- [22] Patrick Esser, Robin Rombach, and Björn Ommer. A disentangling invertible interpretation network for explaining latent representations. In *IEEE Conf. Comput. Vis. Pattern Recog.*, pages 9220–9229, 2020. [2](#)
- [23] Chelsea Finn, Ian J. Goodfellow, and Sergey Levine. Unsupervised learning for physical interaction through video prediction. In Daniel D. Lee, Masashi Sugiyama, Ulrike von Luxburg, Isabelle Guyon, and Roman Garnett, editors, *Advances in Neural Information Processing Systems 29: Annual Conference on Neural Information Processing Systems 2016, December 5-10, 2016, Barcelona, Spain*, pages 64–72, 2016. [2](#)
- [24] Jean-Yves Franceschi, Edouard Delasalles, Mickael Chen, Sylvain Lamprier, and P. Gallinari. Stochastic latent residual video prediction. 2020. [2](#), [6](#), [7](#), [8](#), [13](#), [19](#)
- [25] Hang Gao, Huazhe Xu, Qi-Zhi Cai, Ruth Wang, Fisher Yu, and Trevor Darrell. Disentangling propagation and generation for video prediction. In *Proceedings of the IEEE/CVF International Conference on Computer Vision (ICCV)*, October 2019. [2](#)
- [26] Ishaaq Gulrajani, Faruk Ahmed, Martín Arjovsky, Vincent Dumoulin, and Aaron C. Courville. Improved training of wasserstein gans. In Isabelle Guyon, Ulrike von Luxburg, Samy Bengio, Hanna M. Wallach, Rob Fergus, S. V. N. Vishwanathan, and Roman Garnett, editors, *Adv. Neural Inform. Process. Syst.*, pages 5767–5777, 2017. [17](#)
- [27] Zekun Hao, Xun Huang, and Serge Belongie. Controllable video generation with sparse trajectories. In *IEEE Conf. Comput. Vis. Pattern Recog.*, 2018. [2](#), [7](#), [15](#), [19](#)

- [28] Kaiming He, Xiangyu Zhang, Shaoqing Ren, and Jian Sun. Deep residual learning for image recognition. In *IEEE Conf. Comput. Vis. Pattern Recog.*, pages 770–778, 2016. [4](#), [17](#), [18](#)
- [29] E. Ilg, N. Mayer, T. Saikia, M. Keuper, A. Dosovitskiy, and T. Brox. Flownet 2.0: Evolution of optical flow estimation with deep networks. In *IEEE Conference on Computer Vision and Pattern Recognition (CVPR)*, Jul 2017. [5](#)
- [30] Catalin Ionescu, Dragos Papava, Vlad Olaru, and Cristian Sminchisescu. Human3.6m: Large scale datasets and predictive methods for 3d human sensing in natural environments. *IEEE Transactions on Pattern Analysis and Machine Intelligence*, 36(7):1325–1339, jul 2014. [6](#), [7](#), [8](#), [13](#), [18](#), [19](#)
- [31] Phillip Isola, Jun-Yan Zhu, Tinghui Zhou, and Alexei A. Efros. Image-to-image translation with conditional adversarial networks. In *IEEE Conf. Comput. Vis. Pattern Recog.*, pages 5967–5976, 2017. [18](#)
- [32] Jörn-Henrik Jacobsen, Arnold W. M. Smeulders, and Edouard Oyallon. i-revnet: Deep invertible networks. In *Int. Conf. Learn. Represent.*, 2018. [2](#), [5](#)
- [33] Justin Johnson, Alexandre Alahi, and Li Fei-Fei. Perceptual losses for real-time style transfer and super-resolution. In Bastian Leibe, Jiri Matas, Nicu Sebe, and Max Welling, editors, *Eur. Conf. Comput. Vis.*, pages 694–711, 2016. [17](#)
- [34] Will Kay, João Carreira, Karen Simonyan, Brian Zhang, Chloe Hillier, Sudheendra Vijayanarasimhan, Fabio Viola, Tim Green, Trevor Back, Paul Natsev, Mustafa Suleyman, and Andrew Zisserman. The Kinetics human action video dataset. *CoRR*, 2017. [7](#)
- [35] Diederik P. Kingma and Jimmy Ba. Adam: A method for stochastic optimization. In Yoshua Bengio and Yann LeCun, editors, *Int. Conf. Learn. Represent.*, 2015. [18](#)
- [36] Diederik P. Kingma and Jimmy Ba. Adam: A method for stochastic optimization. In *3rd International Conference on Learning Representations, ICLR 2015, San Diego, CA, USA, May 7-9, 2015, Conference Track Proceedings*, 2015. [18](#), [20](#)
- [37] Durk P Kingma and Prafulla Dhariwal. Glow: Generative flow with invertible 1x1 convolutions. In S. Bengio, H. Wallach, H. Larochelle, K. Grauman, N. Cesa-Bianchi, and R. Garnett, editors, *Advances in Neural Information Processing Systems*, 2018. [2](#), [5](#), [18](#)
- [38] Diederik P. Kingma and Max Welling. Auto-encoding variational bayes. In Yoshua Bengio and Yann LeCun, editors, *Int. Conf. Learn. Represent.*, 2014. [3](#), [4](#), [17](#), [19](#)
- [39] Manoj Kumar, Mohammad Babaeizadeh, Dumitru Erhan, Chelsea Finn, Sergey Levine, Laurent Dinh, and Durk Kingma. Videoflow: A conditional flow-based model for stochastic video generation. In *Int. Conf. Learn. Represent.*, 2020. [2](#)
- [40] Alex X. Lee, Richard Zhang, Frederik Ebert, Pieter Abbeel, Chelsea Finn, and Sergey Levine. Stochastic adversarial video prediction. *Eur. Conf. Comput. Vis.*, 2018. [2](#), [3](#), [7](#), [8](#), [19](#)
- [41] Jae Hyun Lim and Jong Chul Ye. Geometric gan, 2017. [17](#)
- [42] Wen Liu, Zhixin Piao, Jie Min, Wenhan Luo, Lin Ma, and Shenghua Gao. Liquid warping gan: A unified framework for 061431human motion imitation, appearance transfer and novel view synthesis. In *Proceedings of the IEEE/CVF International Conference on Computer Vision (ICCV)*, October 2019. [6](#), [7](#), [8](#), [13](#), [14](#), [18](#)
- [43] Yu-Lun Liu, Yi-Tung Liao, Yen-Yu Lin, and Yung-Yu Chuang. Deep video frame interpolation using cyclic frame generation. In *Proceedings of the 33rd Conference on Artificial Intelligence (AAAI)*, 2019. [2](#)
- [44] Z. Liu, R. A. Yeh, X. Tang, Y. Liu, and A. Agarwala. Video frame synthesis using deep voxel flow. In *2017 IEEE International Conference on Computer Vision (ICCV)*, 2017. [2](#)
- [45] C. Lu, M. Hirsch, and B. Schölkopf. Flexible spatio-temporal networks for video prediction. In *Proceedings IEEE Conference on Computer Vision and Pattern Recognition (CVPR) 2017*, pages 2137–2145. IEEE, 2017. [2](#), [3](#)
- [46] James Lucas, G. Tucker, R. Grosse, and Mohammad Norouzi. Understanding posterior collapse in generative latent variable models. In *DGS@ICLR*, 2019. [20](#)
- [47] Andreas Lugmayr, Martin Danelljan, Luc Van Gool, and Radu Timofte. Srfow: Learning the super-resolution space with normalizing flow. In Andrea Vedaldi, Horst Bischof, Thomas Brox, and Jan-Michael Frahm, editors, *Eur. Conf. Comput. Vis.*, pages 715–732, 2020. [2](#), [18](#)
- [48] Xuezhe Ma, Xiang Kong, Shanghang Zhang, and Eduard Hovy. Macow: Masked convolutional generative flow. 2019. [5](#), [18](#)
- [49] J.G. MacGregor. *An Elementary Treatise on Kinematics and Dynamics*. Macmillan, 1902. [1](#)
- [50] Arun Mallya, Ting-Chun Wang, Karan Sapra, and Ming-Yu Liu. World-consistent video-to-video synthesis. In *CVPR*, 2020. [2](#)
- [51] Michael Mathieu, Camille Couprie, and Yann LeCun. Deep multi-scale video prediction beyond mean square error. 2016. 4th International Conference on Learning Representations, ICLR 2016. [2](#)
- [52] Lars Mescheder, Andreas Geiger, and Sebastian Nowozin. Which training methods for gans do actually converge? In *International Conference on Machine learning (ICML)*, 2018. [17](#)
- [53] Matthias Minderer, Chen Sun, Ruben Villegas, Forrester Cole, Kevin P. Murphy, and Honglak Lee. Unsupervised learning of object structure and dynamics from videos. In *Adv. Neural Inform. Process. Syst.*, pages 92–102, 2019. [2](#), [6](#), [7](#), [13](#)
- [54] Simon Niklaus and Feng Liu. Context-aware synthesis for video frame interpolation. In *IEEE Conf. Comput. Vis. Pattern Recog.*, pages 1701–1710, 2018. [2](#)
- [55] Simon Niklaus and Feng Liu. Softmax splatting for video frame interpolation. In *IEEE Conf. Comput. Vis. Pattern Recog.*, pages 5436–5445, 2020. [2](#)
- [56] George Papamakarios, Eric T. Nalisnick, Danilo Jimenez Rezende, Shakir Mohamed, and Balaji Lakshminarayanan. Normalizing flows for probabilistic modeling and inference. *CoRR*, 2019. [4](#), [18](#)
- [57] Adam Paszke, Sam Gross, Francisco Massa, Adam Lerer, James Bradbury, Gregory Chanan, Trevor Killeen, Zeming Lin, Natalia Gimelshein, Luca Antiga, Alban Desmaison, Andreas Kopf, Edward Yang, Zachary DeVito, Martin Raison, Alykhan Tejani, Sasank Chilamkurthy, Benoit Steiner, Lu Fang, Junjie Bai, and Soumith Chintala. Pytorch: An imperative style, high-performance deep learning library. In *Adv. Neural Inform. Process. Syst.*, pages 8024–8035. 2019. [17](#)

- [58] Albert Pumarola, Stefan Popov, Francesc Moreno-Noguer, and Vittorio Ferrari. C-flow: Conditional generative flow models for images and 3d point clouds. In *IEEE Conf. Comput. Vis. Pattern Recog.*, pages 7946–7955, 2020. [2](#)
- [59] Fitsum Reda, Guilin Liu, Kevin Shih, Robert Kirby, Jon Barker, David Tarjan, Andrew Tao, and Bryan Catanzaro. *SDC-Net: Video Prediction Using Spatially-Displaced Convolution*. 2018. [2](#)
- [60] Danilo Jimenez Rezende and Shakir Mohamed. Variational inference with normalizing flows. In Francis R. Bach and David M. Blei, editors, *International Conference on Machine Learning*, pages 1530–1538, 2015. [2, 18](#)
- [61] Danilo Jimenez Rezende, Shakir Mohamed, and Daan Wierstra. Stochastic backpropagation and approximate inference in deep generative models. In *International Conference on Machine Learning*, pages 1278–1286, 2014. [3, 17, 19](#)
- [62] Robin Rombach, Patrick Esser, and Björn Ommer. Network fusion for content creation with conditional inns. *CoRR*, 2020. [2, 4, 5](#)
- [63] Robin Rombach, Patrick Esser, and Björn Ommer. Network-to-network translation with conditional invertible neural networks. In *Adv. Neural Inform. Process. Syst.*, 2020. [2, 5, 16, 17](#)
- [64] Aliaksandr Siarohin, Stéphane Lathuilière, Sergey Tulyakov, Elisa Ricci, and Nicu Sebe. First order motion model for image animation. In *Adv. Neural Inform. Process. Syst.*, pages 7135–7145, 2019. [6, 7, 8, 13, 18](#)
- [65] Kihyuk Sohn, Honglak Lee, and Xinchen Yan. Learning structured output representation using deep conditional generative models. In *Advances in Neural Information Processing Systems*. Curran Associates, Inc., 2015. [3, 17](#)
- [66] Ke Sun, Bin Xiao, Dong Liu, and Jingdong Wang. Deep high-resolution representation learning for human pose estimation. In *IEEE Conf. Comput. Vis. Pattern Recog.*, pages 5693–5703. Computer Vision Foundation / IEEE, 2019. [7, 8](#)
- [67] Christian Szegedy, Vincent Vanhoucke, Sergey Ioffe, Jonathon Shlens, and Zbigniew Wojna. Rethinking the inception architecture for computer vision. In *IEEE Conf. Comput. Vis. Pattern Recog.*, pages 2818–2826, 2016. [7](#)
- [68] Thomas Unterthiner, Sjoerd van Steenkiste, Karol Kurach, Raphaël Marinier, Marcin Michalski, and Sylvain Gelly. Towards accurate generative models of video: A new metric & challenges. *CoRR*, 2018. [7, 20](#)
- [69] Sjoerd van Steenkiste, Michael Chang, Klaus Greff, and Jrgen Schmidhuber. Relational neural expectation maximization: Unsupervised discovery of objects and their interactions. In *International Conference on Learning Representations*, 2018. [2](#)
- [70] Ruben Villegas, Jimei Yang, Seunghoon Hong, Xunyu Lin, and Honglak Lee. Decomposing motion and content for natural video sequence prediction. In *Int. Conf. Learn. Represent.*, 2017. [2, 13](#)
- [71] Carl Vondrick, Hamed Pirsiavash, and Antonio Torralba. Generating videos with scene dynamics. In *Proceedings of the 30th International Conference on Neural Information Processing Systems*, page 613621, 2016. [2](#)
- [72] Ting-Chun Wang, Ming-Yu Liu, Jun-Yan Zhu, Andrew Tao, Jan Kautz, and Bryan Catanzaro. High-resolution image synthesis and semantic manipulation with conditional gans. In *IEEE Conf. Comput. Vis. Pattern Recog.*, pages 8798–8807, 2018. [17](#)
- [73] Ting-Chun Wang, Ming-Yu Liu, Jun-Yan Zhu, Nikolai Yakovenko, Andrew Tao, Jan Kautz, and Bryan Catanzaro. Video-to-video synthesis. In *Adv. Neural Inform. Process. Syst.*, pages 1152–1164, 2018. [2, 4, 17](#)
- [74] Tsun-Hsuan Wang, Yen-Chi Cheng, Chieh Hubert Lin, Hwann-Tzong Chen, and Min Sun. Point-to-point video generation. In *Proceedings of the IEEE/CVF International Conference on Computer Vision (ICCV)*, October 2019. [2](#)
- [75] Dirk Weissenborn, Oscar Täckström, and Jakob Uszkoreit. Scaling autoregressive video models. In *Int. Conf. Learn. Represent.*, 2020. [2](#)
- [76] Nevan Wichers, Ruben Villegas, Dumitru Erhan, and Honglak Lee. Hierarchical long-term video prediction without supervision. In Jennifer G. Dy and Andreas Krause, editors, *Proceedings of the 35th International Conference on Machine Learning, ICML*, 2018. [2, 6, 13](#)
- [77] Yue Wu, Rongrong Gao, Jaesik Park, and Qifeng Chen. Future video synthesis with object motion prediction. In *IEEE Conf. Comput. Vis. Pattern Recog.*, pages 5538–5547, 2020. [2, 3](#)
- [78] Yuxin Wu and Kaiming He. Group normalization. In Vittorio Ferrari, Martial Hebert, Cristian Sminchisescu, and Yair Weiss, editors, *Eur. Conf. Comput. Vis.*, pages 3–19, 2018. [17, 18](#)
- [79] Tianfan Xue, Baian Chen, Jiajun Wu, Donglai Wei, and William T Freeman. Video enhancement with task-oriented flow. *International Journal of Computer Vision (IJCV)*, 127(8):1106–1125, 2019. [2](#)
- [80] Xinchen Yan, Jimei Yang, Kihyuk Sohn, and Honglak Lee. Attribute2image: Conditional image generation from visual attributes. In Bastian Leibe, Jiri Matas, Nicu Sebe, and Max Welling, editors, *Eur. Conf. Comput. Vis.*, pages 776–791, 2016. [4](#)
- [81] Ceyuan Yang, Zhe Wang, Xinge Zhu, Chen Huang, Jianping Shi, and Dahua Lin. Pose guided human video generation. In *Proceedings of the European Conference on Computer Vision (ECCV)*, September 2018. [2](#)
- [82] Richard Zhang, Phillip Isola, Alexei A. Efros, Eli Shechtman, and Oliver Wang. The unreasonable effectiveness of deep features as a perceptual metric. In *Proceedings of the IEEE Conference on Computer Vision and Pattern Recognition (CVPR)*, June 2018. [7, 20](#)
- [83] Shengjia Zhao, Jiaming Song, and Stefano Ermon. Infovae: Information maximizing variational autoencoders. *CoRR*, 2017. [3, 20](#)
- [84] Zhou Wang, A. C. Bovik, H. R. Sheikh, and E. P. Simoncelli. Image quality assessment: from error visibility to structural similarity. *TIP*, 2004. [7](#)
- [85] Jun-Yan Zhu, Richard Zhang, Deepak Pathak, Trevor Darrell, Alexei A. Efros, Oliver Wang, and Eli Shechtman. Toward multimodal image-to-image translation. In *Adv. Neural Inform. Process. Syst.*, pages 465–476, 2017. [7](#)